

cal convergence zone ( $\approx 11^\circ\text{N}$ ) to values as high as 800 pptv near  $45^\circ\text{N}$ , averaging 26 pptv per  $10^\circ$  of latitude and a mean hemispheric ratio of 1.25 (21). Furthermore, OCS concentrations correlated significantly with those of CO and  $\text{CH}_4$ . Although these results might be interpreted as indicating a seasonal variation caused by uptake of OCS by vegetation in the summer in the Southern Hemisphere, the large and variable values in the Northern Hemisphere may also be interpreted as indicating continental sources of OCS, largely anthropogenic. Additional measurements of the interhemispheric difference in OCS levels, preferably as a function of altitude, will be important in assessing the possible importance of the anthropogenic component.

In addition to possible increases in anthropogenic OCS emissions, the average global surface air temperature increase of about  $0.25^\circ\text{C}$  in the last 30 years (22) may have resulted in increased emissions from natural biogenic sulfur sources. If true, this change represents another perturbation to the global atmosphere associated with increases in greenhouse gases. In any case, a reanalysis of sulfur emission history and the stratospheric chemistry involved should be undertaken. Anthropogenic  $\text{SO}_2$  emissions should not be overlooked; although only a few percent of surface emissions reach the stratosphere, those emissions may be 50 times that of OCS (23). Increased use of current air lanes near the tropopause and anticipated future use of the stratosphere for air travel present sulfur sources that could be more important than previously assumed.

#### REFERENCES AND NOTES

- H. M. Steele and P. Hamill, *J. Aerosol Sci.* **12**, 517 (1981).
- C. E. Junge, C. W. Chagnon, J. E. Manson, *J. Meteorol.* **18**, 81 (1961).
- P. J. Crutzen, *Geophys. Res. Lett.* **3**, 73 (1976).
- E. C. Y. Inn, J. F. Vedder, B. J. Tyson, D. O'Hara, *ibid.* **6**, 191 (1979).
- R. Zander *et al.*, *J. Geophys. Res.* **93**, 1669 (1988).
- O. B. Toon, R. P. Turco, P. Hamill, C. S. Kiang, R. C. Whitten, *J. Atmos. Sci.* **36**, 718 (1979).
- R. P. Turco *et al.*, *ibid.*, p. 699.
- M. A. K. Khalil and R. A. Rasmussen, *Atmos. Environ.* **18**, 1805 (1984).
- D. J. Hofmann and S. Solomon, *J. Geophys. Res.* **94**, 5029 (1989).
- D. J. Hofmann and J. M. Rosen, *ibid.* **87**, 11039 (1982).
- , *Science* **208**, 1368 (1980).
- , *J. Atmos. Sci.* **38**, 168 (1981).
- Sci. Event Alert Network (SEAN) Bull.* **13**, No. 12 (1988); *ibid.* **14**, Nos. 5, 6, 7, and 11 (1989).
- J. M. Rosen and D. J. Hofmann, *J. Appl. Meteorol.* **16**, 56 (1977).
- D. J. Hofmann, J. M. Rosen, W. Gringel, *J. Geophys. Res.* **90**, 2341 (1985).
- D. J. Hofmann, J. M. Rosen, J. W. Harder, S. R. Rolf, *Geophys. Res. Lett.* **14**, 614 (1987).
- D. J. Hofmann and T. Deshler, *ibid.* **16**, 1429 (1989).
- W. A. Sedlacek, E. J. Mroz, A. L. Lazrus, B. W. Gandrud, *J. Geophys. Res.* **88**, 3741 (1983).
- R. G. Pinnick *et al.*, *J. Atmos. Sci.* **33**, 304 (1976).
- A. L. Torres, P. J. Maroulis, A. B. Goldberg, A. R. Bandy, *J. Geophys. Res.* **85**, 7357 (1980).
- H. G. Bingemer, S. Burgermeister, R. L. Zimmermann, H.-W. Georgii, *ibid.*, in press.
- J. F. B. Mitchell, *Rev. Geophys.* **27**, 115 (1989).
- R. P. Turco *et al.*, *Nature* **283**, 283 (1980).
- This research was supported by the Atmospheric Chemistry Section of the National Science Foundation.

20 November 1989; accepted 14 March 1990

## Faults in the Mojave Desert, California, as Revealed on Enhanced Landsat Images

J. P. FORD, R. K. DOKKA, R. E. CRIPPEN, R. G. BLOM

Previously unknown strike-slip and normal faults in the central and eastern Mojave Desert have been revealed on Landsat Thematic Mapper images enhanced by four-component processing. This method provides color images on which lithologies are discriminated by their contrasting absorption and reflection, primarily at infrared wavelengths and particularly with regard to their ferric iron, ferrous iron, and hydroxyl contents, while retaining landform depiction. These discriminants represent a new type of geophysical display for geologic mapping in regions of well-exposed bedrock. Faults are revealed on the images by abrupt spectral and textural contrasts that coincide with aligned topographic features. The newly discovered faults form part of an extensive regional network of right shear that connects faults in the Death Valley region with the San Andreas fault system. They support a heterogeneous strain model for late Cenozoic tectonic evolution of the region. Regional structural relations indicate a westward migration of the locus of strain through time. Some of the newly identified faults bound blocks that have experienced contrasting rotational histories since early Miocene time.

THE MOJAVE DESERT BLOCK (MDB) tectonic unit in Southern California has had a complex history of late Cenozoic deformation. The block covers  $\sim 38,000 \text{ km}^2$  at the western margin of the North American Plate. It is bounded by the San Andreas fault zone to the southwest, the Pinto Mountain fault to the south, the Garlock fault to the north, and the Granite Mountains fault to the east (1) (Fig. 1). The MDB is thought to have been deformed under two different tectonic regimes in late Cenozoic time. Early Miocene extensional tectonism in the Mojave (2, 3) was followed by dominantly northwest-striking, right-slip faulting that began after 13 Ma (million years ago) (1, 4). Paleomagnetic evidence suggests that both regimes were accompanied by block rotations (5–7). The MDB is broken internally by many subparallel strike-slip faults 10 to 20 km apart. Dibblee (8) recognized the right-slip character of these faults and their likely relationship to the San Andreas fault system. Subsequent tectonic models held that the faults resulted from simple shear that was regionally distributed across the MDB in late Cenozoic time, but the details of timing and fault development

were not well understood (9). These faults are important because of their dominant role in establishing the present structural and physiographic grain of the MDB and for the seismic hazard that they represent (10).

About 50% of the surface area of the MDB consists of alluviated basins and associated dry lake beds (11). Although vegetative cover is sparse ( $< 10\%$ ), the geology of the basins and alluviated surfaces is poorly known and largely generalized on the basis of reconnaissance mapping (1:62,500 or smaller). One reason is that much of the MDB is difficult of access or is closed to the public. Also, alluvium and dry lake deposits cover the bedrock geology in key areas. Images obtained at multiple wavelengths by the earth-orbiting Landsat Thematic Mapper (TM) system are suitable for regional and local analyses and provide map scale data that are not available from other sources.

We have used Landsat TM, aerial photographs, and other types of images to study  $\sim 2000 \text{ km}^2$  in the central and eastern MDB, where little detailed mapping is available. Landsat TM images processed by a four-component technique have provided valuable spectral information that reveals contrasting compositional characteristics of the rocks mostly at infrared wavelengths, while retaining landform depiction. Such

J. P. Ford, R. E. Crippen, R. G. Blom, Jet Propulsion Laboratory, Mail Stop 300/233, Pasadena, CA 91109.  
R. K. Dokka, Louisiana State University, Department of Geology and Geophysics, Baton Rouge, LA 70803.

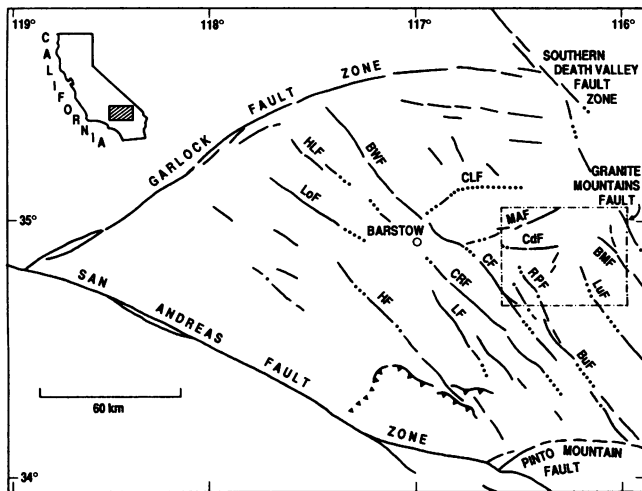


**Fig. 1.** Outline of MDB showing major faults and limits of study area at east center. BuF, Bullion fault; BMF, Bristol Mountains fault; BWF, Blackwater fault; CF, Calico fault; CdF, Cady fault; CLF, Coyote Lake fault; CRF, Camp Rock fault; HF, Helendale fault; HLF, Harper Lake fault; LF, Lenwood fault; LuF, Ludlow fault; MAF, Manix-Afton fault; RPF, Rodman-Pisgah fault.

images have proved to be more helpful in detecting previously unknown faults and guiding field investigations than other types of remote sensing data. The enhanced TM images used in this study are in marked contrast with low-resolution, single-band, and other types of false-color displays that reveal little more about lithologies and structures than is conveyed by the landforms.

The study area is located ~60 km east of Barstow, California, and includes the Cady Mountains, northern Bristol Mountains, and adjacent alluviated lowlands (Fig. 2). Published geologic maps of this area include small-scale reconnaissance maps (12, 13), two full 15' quadrangles (14), and segments of four adjacent quadrangles to the west and south (15). Rocks of the region consist of Mesozoic granitoids, moderate to steeply dipping upper Oligocene through middle Miocene volcanic rocks, and younger, gently dipping nonmarine deposits (16). Late Tertiary and Quaternary basaltic lavas cover some areas. Alluvial gravels, sands, and clays are exposed in the valleys, canyons, and dry lakes. Eolian sand deposits are widespread.

The area is cut by strike-slip faults with differing orientations and directions of movement. The eastern half of the area is characterized by right-slip faults that mostly strike northwest and terminate in the northern part of the area. To the west in the Cady Mountains, northeast- to east-striking left-slip faults are prominent and are associated with pull-apart basins and differentially rotated blocks (4, 7). Faults south and southwest of the Cady Mountains strike northwest and display right-slip offsets similar to the faults in the east. All the strike-slip faults in the area are considered to be younger than 13 Ma (4).

Landsat TM data obtained in summer (28 July 1985) at a relatively high sun-elevation angle of 58° were used for this study. The

data were processed to enhance the surface spectral responses in a color-composite image (Fig. 2) without suppressing the topography (17). This was achieved by means of a four-component processing technique. Each of three band ratio channels was modulated by the band-average reflectivity, and then assigned different primary colors. The infrared (IR) and visible wavelength TM band ratios used (5/7, 5/4, and 3/1) emphasize compositional differences of the rocks (18).

High values for band ratio 5/7 (depicted as red) generally denote  $\text{OH}^+$  rich minerals, high values for band ratio 5/4 (depicted as green) generally denote rocks rich in  $\text{Fe}^{2+}$ , and high values for band ratio 3/1 (depicted as blue) generally denote rocks rich in  $\text{Fe}^{3+}$ . The band average information primarily enhances topographic features. Thus, four dimensions of data are displayed simultaneously in a readily interpretable fashion in the image. Potential confusion of these four dimensions in three-dimensional color space is minimized because the spatial differences between topographic and reflectance information are commonly distinct. These enhancement procedures reveal important geologic information that is not apparent in the single-band black-and-white images or in standard false-color-composite images made from the same TM data set.

The color patterns in the TM image provide contrasting compositional information mostly at IR wavelengths. These patterns allow the discrimination and mapping of many types of surface materials that do not display strong visible color contrasts. In many cases, the color contrasts (hence compositional differences) seen in the image (Fig. 2) allow the detection of features overlooked in conventional field mapping. Gra-

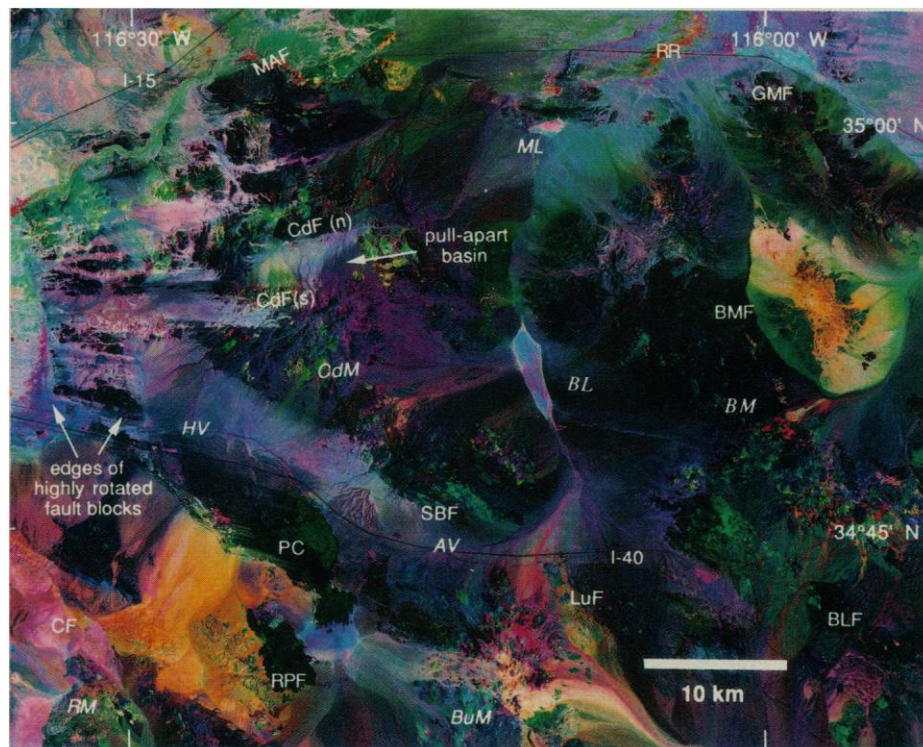


**Fig. 2.** Landsat TM color-composite band-ratio image of eastern Mojave Desert. Newly discovered faults: BLF, Broadwell Lake fault; CdF (n), Cady fault north strand; and SBF, Sleeping Beauty fault. Previously documented faults: BMF, Bristol Mountains fault; CF, Calico fault; CdF (s), Cady fault south strand; GMF, Granite Mountains fault; LuF, Ludlow fault; MAF, Manix-Afton fault; and RPF, Rodman-Pisgah fault. Prominent features: PC, Pisgah Crater; BL, Broadwell Lake; ML, Mesquite Lake; BM, Bristol Mountains; BuM, Bullion Mountains; CM, Cady Mountains; RM, Rodman Mountains; AV, Argos Valley; HV, Hector Valley; I, interstate; RR, railroad.

nitic rocks appear in shades of pink, red, or pale blue in the image. Less siliceous diorite, andesite, andesitic fanglomerate, and volcanoclastic rocks such as tuff breccia range from green and yellowish green to dark greenish brown. Basalt ranges from green and dark green to cyan. Alluvial deposits in the lowlands commonly appear in distinctive shades of color that point to the matching source areas. Highly reflective lake bed deposits and windblown sand appear white to pink or pale blue. Faults are seen in the image as aligned topographic features that coincide with abrupt linear color or textural discontinuities [for example, Fig. 2, Granite Mountains fault, Bristol Mountains fault, Ludlow fault, and Cady fault (south strand)]. The color balance is set for maximal discrimination of the scene materials and is therefore somewhat scene-dependent. Intensity variations in the image enhance the detection of topographic features that are indicative of rock types as well as structures.

Image analysis and directed field checking have resulted in the discovery of previously unknown faults and related structures in the area. The Broadwell Lake fault is denoted by a prominent discontinuous alignment of tuffs and tuff breccias (brown) and basaltic or andesitic rocks (green and greenish blue) in the TM image (Fig. 3). This fault strikes northwest for about 25 km in the Bristol Mountains, through Black Ridge to the Lava Hills. The fault is not obvious in aerial photographs and radar images, which emphasize topography, and it cannot be traced into Broadwell Lake to the northwest or beyond the Lava Hills to the southeast. The fault identified on the image was examined and confirmed in the field. Fault gouge and caliche are exposed discontinuously along it. At its most northwesterly exposure it strikes  $325^{\circ}\text{W}$ , dips moderately northeastward, and has down-dip slickensides indicative of dip-slip motion. About 13 km southeast, south of Black Ridge in Siberia Wash the fault strikes  $315^{\circ}$ , is subvertical, and has subhorizontal slickensides indicative of strike-slip motion. Although the fault is located in a broad zone of right-slip movement, piercing points have not yet been located in the field that would constrain the direction and amount of displacement that has occurred. Undeformed Pleistocene alluvial gravels unconformably overlie the faulted bedrock in some of the washes (Fig. 3C); thus the fault has not been recently active.

The previously documented east-striking Cady fault (13) is well marked in the image as is a newly located subparallel fault strand that lies 1 to 3 km to the north and extends to the east-northeast for about 10 km (Fig. 3E). We designate the known Cady fault as the Cady fault–south strand; the newly lo-

cated (and field-verified) fault is the Cady fault–north strand. The wide depression (Hidden Valley) that connects the eastern part of the southern strand to the western end of the northern strand appears to be a pull-apart basin formed along a single, left-stepping, left-slip fault system, as suggested by Dokka and Travis (4).

In the southwest and central Cady Mountains, highly rotated fault blocks of basaltic to andesitic breccias and tuffs described by Ross *et al.* (7) appear reddish brown on the TM image (Fig. 2). Some of the blocks show linear margins up to 3 km in length that range in orientation from northeast to northwest. Such margins probably represent faults associated with the block rotations. An example north of Hidden Valley exposes a steeply inclined northeast-oriented fault plane with down-dip slickensides indicative of dip slip motion (Fig. 3D).

In the south Cady Mountains, the Sleeping Beauty fault (SBF) (4) is marked in the TM image (Fig. 2) by a discontinuous curvilinear alignment of andesitic and basaltic rocks (green to greenish blue) and aligned outcrops of eroded older fanglomerates (pink to pale blue) between the mountain front and the Pisgah lava flow (dark green). This fault extends east-southeast for about 14 km. Field evidence for this now buried

fault includes the alignment of truncated spurs (4, 13) and the geometry of shortening structures in Miocene through Quaternary strata along the southern Cady Mountains. The orientation of these faults and folds relative to the east-southeast-trending line of truncated spurs is suggestive of a left-slip component of movement on the SBF (4).

The faults described above are interpreted as part of a regional network of right shear that connects the Death Valley region with the San Andreas fault system. Because of this physical connection it is probable that this regional network has accommodated a significant fraction of Pacific–North American plate motion since middle Miocene time. Structural relationships along the faults suggest at least two intervals of movement. Faults located east of Broadwell Lake are overlain by unconsolidated alluvial fan debris and are probably inactive. In contrast, the area to the west (Cady Mountains) contains faults that cut all deposits and is seismically active. The present pattern of faulting and strain indicates that regional shear is now concentrated in the central and southern parts of the MDB (19). This westward shift of activity may have occurred between 1.5 and 0.7 Ma (4).

Dokka and Travis have suggested that strain across the MDB since middle Mio-

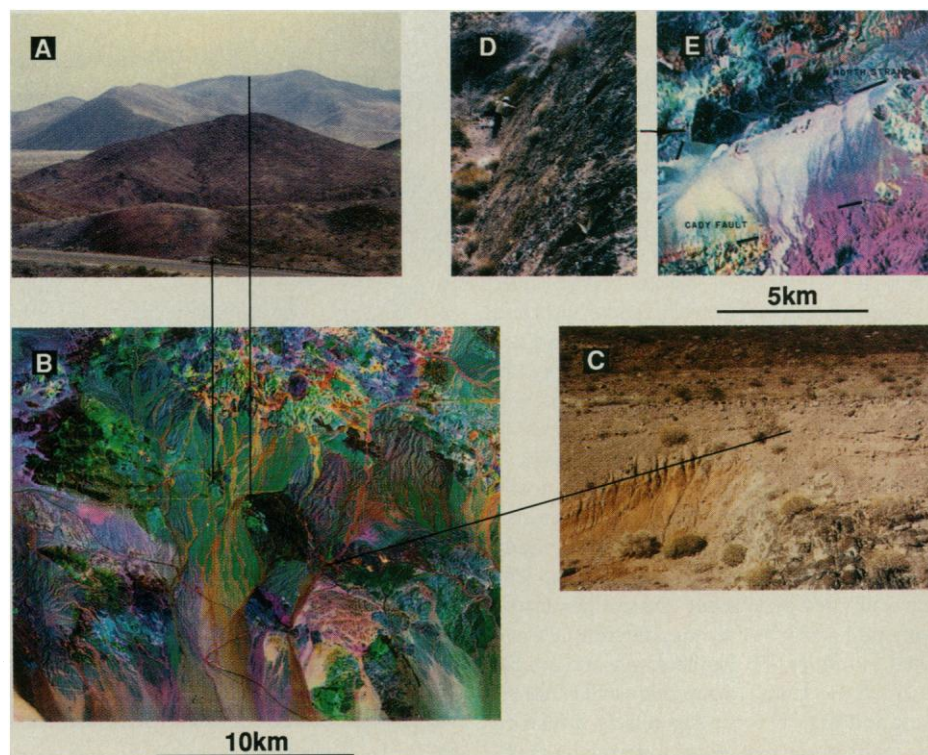


**Fig. 3.** The Broadwell Lake fault shows (A) lack of distinctive topography at Black Ridge, (B) pronounced alignment of discontinuous rock outcrops from upper left to lower right on TM image (enlarged from Fig. 2), and (C) fault contact overlain by undisturbed late Pleistocene and Holocene gravels at Siberia Wash. High-angle normal fault (D) in tuff breccia north of Hidden Valley dips  $\sim 55^{\circ}$  southeast exposing  $\sim 8$  m scarp and down dip slickensides. The Cady fault shows (E) north and south fault strands with pull-apart basin (enlarged from Fig. 2).

cene time is regionally heterogeneous and is partitioned into six domains that have independent histories and styles of late Cenozoic deformation (4). These domains are separated by zones of extension and strike slip. Tectonic rotation and internal deformation of the MDB domains are regarded as produced within a belt of regionally distributed right shear that Dokka and Travis termed the Eastern California shear zone. At least 65 km of right slip is believed to have occurred across this zone; this accounts for 9 to 14% of the motion between the North American and Pacific plates since 10.6 Ma (4). Because of kinematic and temporal similarities, this shear zone is thought also to include the southern Death Valley and the adjacent Furnace Creek fault zones (Fig. 1).

This heterogeneous strain model is based on field mapping, which shows that most northwest-striking faults in the MDB lack continuity across the block; that with only one exception the faults fall into two distinct groups separated across an east-oriented strip of terrain that passes through Barstow; and that there is a major discrepancy in the slip values on individual faults to the south and their projected counterparts to the north. This model differs substantially from regionally distributed simple shear models (9) that require continuity of the faults, and uniform slip across the entire MDB.

The newly observed faults provide supporting evidence for the heterogeneous strain model. The Broadwell Lake fault is limited in extent, in common with other right-slip faults in the area to the northeast (Bristol Mountains and Granite Mountains faults) and west (Ludlow fault). The fault is situated in an area of dominant right shear that reportedly shows no evidence of rotation (20). A net slip of 0.5 km is predicted for this fault from the combined right-slip offset that is believed to have been accommodated since 10 Ma in the central and eastern Mojave Desert. The model also predicts about 35 km of late Cenozoic right shear along the nearby Bristol Mountains and Granite Mountains faults.

The Cady Mountains and the SBF are situated in an area of dominant left slip. The SBF marks the southern limit of this area, as predicted by the heterogeneous strain model. Paleomagnetic declination studies from the Cady Mountains indicate contrasting rotations of crustal blocks in this region. Whereas most blocks were rotated clockwise an average of  $\sim 50^\circ$  prior to about 18 Ma, the southwest Cady Mountains appear to have rotated about  $124^\circ$  clockwise (7). Deformation during rotation was accomplished in part by left-slip motion on a number of internal faults that include the north strand of the Cady fault.

In summary, the enhanced TM images have allowed the recognition of important faults overlooked by field geologists, the field investigation of faults so recognized, the regional analysis of their significance, and the associated implications for models of tectonic evolution in the MDB. These results show effective use of multispectral image analysis for tectonic studies in complexly deformed terrain at local and regional map scales. They also show that previous mapping of faults in the study area was inadequately representative. Continued field mapping guided by remote sensing image analyses over wider areas of the Mojave Desert can improve understanding of deformation in this region.

#### REFERENCES AND NOTES

1. R. K. Dokka, *Geology* **11**, 305 (1983); —, M. McCurry et al., in *This Extended Land, Geological Journeys in the Southern Basin and Range*, D. L. Weide and M. L. Faber, Eds., *Geol. Soc. Am. Cordilleran Sect. Field Trip Guidebook* (Department of Geoscience, University of Nevada, Las Vegas, NV, 1988), pp. 21–44.
2. R. K. Dokka, *Geol. Soc. Am. Spec. Pap.* **208**, 75 (1986); — and M. O. Woodburne, *Louisiana State Univ. Publ. Geol. Geophys. Tecton. Sediment.* **1** (1986); A. F. Glazner, J. M. Bartley, J. D. Walker, *Geology* **17**, 50 (1989).
3. R. K. Dokka, *Tectonics* **8**, 363 (1989).
4. — and C. J. Travis, *ibid.*, **9**, 311 (1990).
5. M. Golombek and L. Brown, *Geology* **16**, 126 (1988).
6. B. J. McFadden, M. O. Woodburne, N. D. Opdyke, *J. Geophys. Res.* **95**, 4597 (1990).
7. T. M. Ross, B. P. Luyendyk, R. B. Haston, *Geology* **17**, 470 (1989); T. M. Ross and R. K. Dokka, *Geol. Soc. Am. Abstr. Progr.* **22** (no. 3), 79 (1990).
8. T. W. Dibblee, Jr., *U.S. Geol. Surv. Prof. Pap.* **424-B** (1961), p. B107.
9. Z. Garfunkel, *Geol. Soc. Am. Bull.* **85**, 1931 (1974); J. N. Carter et al., *ibid.* **98**, 199 (1987).
10. S. G. Wesnousky, *J. Geophys. Res.* **91**, 12587 (1986).
11. C. W. Jennings (compiler), *Geologic Data Map No. 2*. (Calif. Div. Mines Geol., Sacramento, CA 1977).
12. D. F. Hewett, *Calif. Div. Mines Geol. Bull.* **170** (part 2), 15 (1954).
13. A. M. Bassett and D. H. Kupfer, *Calif. Div. Mines Geol. Spec. Rep.* **83** (1964); plate 1 of Bassett and Kupfer was previously published as *U.S. Geol. Surv. Misc. Inv. Field Studies Map MF-205* (1962). The geology was mapped in 1953.
14. T. W. Dibblee, Jr., *U.S. Geol. Surv. Misc. Geol. Inv. Map I-478* (1967); — and A. M. Bassett, *ibid.* **I-467** (1966); larger scale maps of parts of the area appear in an unpublished survey by the Southern Pacific Minerals Company (now Santa Fe Mining, Inc).
15. T. W. Dibblee, Jr., and A. M. Bassett, *U.S. Geol. Surv. Misc. Geol. Inv. Map I-461* (1966); T. W. Dibblee, Jr., *ibid.*, **I-430** (1964); *ibid.*, **I-472** (1966); *ibid.* **I-477** (1967).
16. D. Miller, K. Howard, B. John, in *Geologic Excursions in the California Desert*, J. D. Cooper, Ed., *Geol. Soc. Am. Cordilleran Sect. Meeting Guidebook* (Pacific Section, Society of Economic Paleontologists and Mineralogists, Bakersfield, CA, 1982), pp. 91–100; M. Woodburne and R. Tedford, *ibid.*, pp. 65–76; A. F. Glazner, *Geol. Soc. Am. Bull.* **100**, 424 (1988); D. Miller, *Geol. Soc. Am. Abstr. Progr.* **20** (no. 3), 215 (1988).
17. R. E. Crippen, Ph.D. thesis, University of California, Santa Barbara (1989).
18. M. H. Podwysocki, M. S. Power, O. D. Jones, *Adv. Space Res.* **5** (no. 5), 13 (1985).
19. D. M. Morton, F. K. Miller, C. C. Smith, *U.S. Geol. Surv. Misc. Field Studies Map MF-1051* (1980); J. Sauber, W. Thatcher, S. Solomon, *J. Geophys. Res.* **91**, 12683 (1986); S. Goter (compiler), *Seismicity of California, 1808–1987*, *U.S. Geol. Surv. Open-File Rep.* **88-286** (1988).
20. R. E. Wells and J. W. Hillhouse, *Geol. Soc. Am. Bull.* **101**, 846 (1989).
21. This research was performed by the Jet Propulsion Laboratory, Pasadena, CA, under contract to the National Aeronautical and Space Administration, Washington, DC. Additional support was provided from a Summer Faculty Fellowship award to R.K.D. under the JPL/Caltech NASA Program. Field investigations by R.K.D. were supported by grants from the National Science Foundation. Discussions with R. H. Brady, G. A. Davis, W. Hamilton, T. M. Ross, C. J. Travis, and M. O. Woodburne were valuable.

18 December 1989; accepted 19 March 1990

## Reversal of Creatine Kinase Translational Repression by 3' Untranslated Sequences

J. LAI C. CH'NG,\* DAVID L. SHOEMAKER, PAUL SCHIMMEL, EDWARD W. HOLMES†

A subline of U937 cells (U937D) was obtained in which creatine kinase B (CK-B) messenger RNA was present and bound to ribosomes, but CK activity was undetectable. Transformation of U937D cells with retrovirus vectors that contain the 3' untranslated region (3' UTR) of CK-B messenger RNA exhibited CK activity with no change in abundance of CK-B mRNA. The 3' UTR formed a complex *in vitro* with a component of S100 extracts from wild-type cells. This binding activity was not detectable in S100 extracts from cells that expressed CK activity after transformation with the 3' UTR-containing vector. These results suggest that translation of CK-B is repressed by binding of a soluble factor or factors to the 3' UTR.

**A** COMMON FEATURE OF EUKARYOTIC mRNAs is a 3' UTR of variable length. In some genes, the primary sequence of the 3' UTR is conserved across

species (1), implying that a function exists for these sequences. Stability of mRNA can be regulated by interaction of the 3' UTR with soluble cellular proteins (2). The 3'